The synthetic double wavelength technique: a simple robust method for thermodynamic temperature determination

Stéphan Briaudeau, Frédéric Bourson, Olga Kozlova, Mohamed Sadli, Annick Razet

Metrologia

The synthetic double wavelength technique: a simple robust method for thermodynamic temperature determination

OPEN ACCESS
IOP Publishing
Metrologia
Metrologia **57** (2020) 025014 (15pp)
https://doi.org/10.1088/1681-7575/ab7173

The synthetic double wavelength technique: a simple robust method for thermodynamic temperature determination

Stéphan Briaudeau, Frédéric Bourson, Olga Kozlova, Mohamed Sadli and Annick Razet

Laboratoire commun de métrologie, LNE-Cnam, Saint Denis, France

E-mail: stephan.briaudeau@lecnam.net

Received 17 October 2019, revised 12 January 2020
Accepted for publication 29 January 2020
Published 27 March 2020

Abstract

This paper describes a new relative technique developed at LNE-Cnam, for the determination of the thermodynamic temperature of blackbodies without recourse to a radiometric reference. This technique is referred to as the 'synthetic double wavelength technique' (SDWT) as it is considered to be a particular case of the 'double wavelength technique' (DWT). It offers a new experimental technique for the determination of the thermodynamic temperature at high temperature and as such a new means for the *mise-en-pratique* of the new definition of the kelvin achievable by any national metrology institute provided a multi-wavelength radiation thermometer combining large and narrow bandwidths is available. In this work, a first experimental implementation of this technique based on a wavelength-tuneable spectroradiometer providing both narrowband and broadband signals with the particularity of the broadband signal being virtually synthesised from the spectral distribution of the narrowband signals sampled over a wide spectral range. SDWT determination of the thermodynamic temperature of a blackbody at 2760 K was performed with a level of uncertainty that confirms the promising capabilities of this technique.

Keywords: temperature unit, kelvin, SI, *mise en pratique*, dissemination, thermodynamic temperature, double wavelength technique

1. Introduction

In the newly redefined International System of Units [1], the unit of thermodynamic temperature, the kelvin, is defined through the fixed value of the Boltzmann constant opening the way for the realisation and dissemination of thermodynamic temperatures over the whole temperature range as stated in the *mise-en-pratique* of the kelvin [2].

Primary radiometric methods developed during the last decades being quite complex for most National Metrology Institutes (NMIs) the idea of using other techniques, not related to the cryogenic radiometer, such as the double wavelength technique or the synchrotron radiation as a calculable reference was proposed and put into application in the frame of the EMPIR project InK2 [3].

This article describes a new and simple technique for the determination of thermodynamic temperature of a blackbody, called 'Synthetic Double Wavelength Technique (SDWT)'. As for the double-wavelength technique (DWT) [4–9], SDWT is based on the ratio of the spectroradiometer signals of two different optical bands (a narrowband, and a broadband) at two different blackbody temperatures (T_1 and T_2). The advantage of the SDWT is that this technique does not require the calibration of the relative spectral responsivity of a broadband optical filter. Instead, the broadband measurement is

constructed with a set of tuned narrow band measurements. Therefore, the synthetic broadband spectral responsivity can be written as a sum of tuned narrowband spectral responsivity. This technique has been successfully tested with two blackbodies at the respective temperatures of 1358 K and 2760 K.

In the second section, the DWT is recalled. Its principle is explained for an ideal case in which narrowband is purely monochromatic and the spectral bandwidth is infinite for broadband measurements (grey spectral responsivity of the instrument measuring blackbody radiance).

In the third section of this article, the principle of SDWT is described using the assumption of purely monochromatic measurement of blackbody radiance used in the narrowband case.

In the fourth section, the temperature of a blackbody is measured according to the International Temperature Scale of 1990 (ITS-90) scheme. Experimental results are presented, and the uncertainty budget is developed, demonstrating the existence of systematic spectral effects originating from the optical instrument, which is a simple-grating Czerny-Turner monochromator-based spectroradiometer (or radiance comparator) used for the measurement of the blackbody radiance.

In the fifth section, experimental determination of the thermodynamic temperatures of two blackbodies using SDWT is detailed. The uncertainty budget is developed, and systematic errors are discussed.

In the sixth section, the systematic errors observed both on the ITS-90-scheme and SDWT experimental results are simulated numerically to check some hypotheses on their physical origins. As a result, part of the systematic effects may be corrected while abrupt spectral variations are still not yet fully understood.

2. Double wavelength technique

2.1. Principle

In a general case, the DWT consists in measuring the radiance of two blackbodies at temperatures T_1 and T_2 with two radiometers or radiation thermometers having different relative spectral responsivities $S_1(\lambda)$ and $S_2(\lambda)$. Total of four radiometer signals $I(T)$ can be expressed as:

$$I_1(T_1) = k_1 \int_0^\infty S_1(\lambda) \cdot L(\lambda, T_1)\, d\lambda \tag{1}$$

$$I_1(T_2) = k_1 \int_0^\infty S_1(\lambda) \cdot L(\lambda, T_2)\, d\lambda \tag{2}$$

$$I_2(T_1) = k_2 \int_0^\infty S_2(\lambda) \cdot L(\lambda, T_1)\, d\lambda \tag{3}$$

$$I_2(T_2) = k_2 \int_0^\infty S_2(\lambda) \cdot L(\lambda, T_2)\, d\lambda \tag{4}$$

where $S_1(\lambda)$ and $S_2(\lambda)$ are the relative spectral responsivities related to the absolute spectral responsivities $k_1 S_1(\lambda)$ and $k_2 S_2(\lambda)$ by the constants k_1 and k_2. $L(\lambda,T)$ is the spectral radiance distribution at a temperature T given by Planck's law:

$$L(\lambda, T) = \frac{C_1}{n^2(\lambda) \cdot \lambda^5} \cdot \left[exp^{\frac{C_2}{n(\lambda)\cdot\lambda\cdot T}} - 1 \right]^{-1} \tag{5}$$

with $C_1 = 1.191042972\,10^{-16}\,\mathrm{W.m^2}$ and $C_2 = 1.438776877\,10^{-2}\,\mathrm{m.K}$, the first and second radiation constants, respectively; the refractive index $n(\lambda)$, which has the following wavelength dependency in its typical measurements conditions (air, visible and near infrared range) [10]:

$$n - 1 = \frac{0.05792105}{238.0185 - \lambda^{-2}} + \frac{0.00167917}{57.362 - \lambda^{-2}} \tag{6}$$

The ratios of the radiometer signals measuring the blackbodies at T_1 and T_2, under the assumption that the effective emissivity of the blackbodies at each wavelength is the same for the two temperatures, can be written as:

$$\beta_1^{exp}(T_1, T_2) = \frac{I_1(T_2)}{I_1(T_1)} \tag{7}$$

$$\beta_1^{model}(T_1, T_2) = \frac{\int_0^\infty S_1(\lambda) \cdot L(\lambda, T_2)\, d\lambda}{\int_0^\infty S_1(\lambda) \cdot L(\lambda, T_1)\, d\lambda} \tag{8}$$

$$\beta_2^{exp}(T_1, T_2) = \frac{I_2(T_2)}{I_2(T_1)} \tag{9}$$

$$\beta_2^{model}(T_1, T_2) = \frac{\int_0^\infty S_2(\lambda) \cdot L(\lambda, T_2)\, d\lambda}{\int_0^\infty S_2(\lambda) \cdot L(\lambda, T_1)\, d\lambda} \tag{10}$$

DWT model gives then a system of two equations which describes respectively the narrowband and the broadband measurement equations with two unknowns T_1 and T_2. As DWT only requires the knowledge of the relative spectral responsivities $S_1(\lambda)$ and $S_2(\lambda)$, this technique is an alternative to complex absolute radiometric methods [11–14], that are traceable to the watt via an electrical substitution cryogenic radiometer [15].

Narrowband radiance ratios measurement equation:

$$\beta_1^{model}(T_1, T_2) = \beta_1^{exp}(T_1, T_2) \tag{11}$$

Broadband radiance ratios measurement equation:

$$\beta_2^{model}(T_1, T_2) = \beta_2^{exp}(T_1, T_2) \tag{12}$$

2.2. Case study: ideal measurement of the radiance of a blackbody

There is an ideal configuration where the solutions of DWT can be computed analytically. The relative spectral responsivity $S_1(\lambda)$ can be considered sufficiently narrow to be expressed with a Dirac δ-distribution centered on optical wavelength λ_m. The relative spectral responsivity $S_2(\lambda)$ is considered sufficiently wide to be approximated by a broadband of infinite bandwidth.

We can therefore introduce the narrowband relative spectral responsivity $S_1(\lambda, \lambda_m)$ centred on the optical wavelength λ_m which replaces the relative spectral responsivity $S_1(\lambda)$ defined by equations (1) and (2).

The narrowband relative spectral responsivity $S_1(\lambda, \lambda_m)$ is then the product of the Dirac δ-distribution and the relative spectral response $R(\lambda)$ of the instrument:

$$S_1(\lambda, \lambda_m) = R(\lambda) \cdot \delta(\lambda - \lambda_m) \tag{13}$$

$$R(\lambda_m) = \int S_1(\lambda, \lambda_m)\, d\lambda \tag{14}$$

With in monochromatic approximation of the narrowband radiance measurement, the photocurrent $I_1(T)$ depends on the measurement optical wavelength λ_m; therefore, it is replaced by $I_1(\lambda_m, T)$:

$$\begin{aligned} I_1(T) \rightarrow I_1(\lambda_m, T) &= k_1 \int_0^\infty S_1(\lambda, \lambda_m) \cdot L(\lambda, \mathrm{T})\, d\lambda \\ &\cong k_1 \cdot R_1(\lambda_m) \cdot L(\lambda_m, \mathrm{T}) \end{aligned} \tag{15}$$

Therefore, the signal ratio $\beta_1^{exp}(T_1, T_2)$ for the narrow band detection depends also on the measurement optical wavelength λ_m: it is then replaced by $\beta_1^{exp}(\lambda_m, T_1, T_2)$:

$$\beta_1^{exp}(T_1, T_2) \rightarrow \beta_1^{exp}(\lambda_m, T_1, T_2) = \frac{I_1(\lambda_m, T_2)}{I_1(\lambda_m, T_1)} \tag{16}$$

For monochromatic measurements the model of the signal ratio (8) depends also on the measurement optical wavelength λ_m. Thus $\beta_1^{model}(T_1, T_2)$ is then replaced by $\beta_1^{model}(\lambda_m, T_1, T_2)$:

$$\beta_1^{model}(T_1, T_2) \rightarrow \beta_1^{model}(\lambda_m, T_1, T_2) \cong \frac{L(\lambda_m, T_2)}{L(\lambda_m, T_1)} \tag{17}$$

In practice, spectral responsivities of narrowband filters are sufficiently narrow to be considered as a Dirac distribution, whereas the broadband measurement can be performed with a spectrally flat thermal photodetection of an infinite optical bandwidth.

Using Wien's approximation $\left(\lambda_m \ll \frac{C_2}{T}\right)$ the narrowband measurement equation (11) becomes:

$$\frac{1}{T_2} \cong \frac{1}{T_1} - \frac{n(\lambda_m) \cdot \lambda_m}{C_2} \cdot ln\left[\beta_1^{exp}(\lambda_m, T_1, T_2)\right] \tag{18}$$

Considering a perfectly flat spectral responsivity of the instrument used for the measurement of blackbody radiance, $S_2(\lambda) = S_2$ as an ideal case, one may apply Stefan Boltzmann's law to the broadband measurement equation (12) which becomes:

$$\frac{1}{T_2} \cong \frac{1}{T_1} \cdot \left[\beta_2^{exp}(T_1, T_2)\right]^{-\frac{1}{4}} \tag{19}$$

Therefore, SDWT provides a two-equations system (18, 19) which may be solved for the analytical expression of the thermodynamic temperatures T_1 and T_2 of the two blackbodies used in measurements.

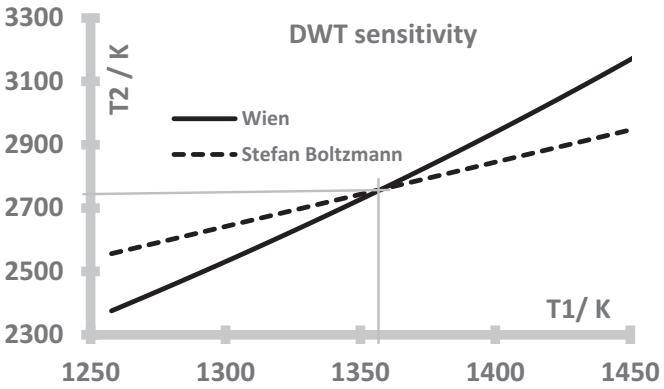

Figure 1. T_1 and T_2 are the solutions of the system equations (18) and (19) for $\lambda_m = 830\,\mathrm{nm}$.

For a graphical illustration, we shall consider the temperatures $T_1 = 1357.8\ K$, $T_2 = 2760.5\ K$ and a monochromatic wavelength $\lambda_m = 830\,\mathrm{nm}$.

Close to their intersection, the two curves defined by the equations (18) and (19) are approximately linear (see figure 1). These curves exhibit very different slopes, which is a consequence of the strong difference of the temperature dependence of the blackbody radiance using Wien's law and Stefan Boltzmann's law.

Thermodynamic blackbody temperature values T_1 and T_2 may also be computed numerically from direct comparison between the model and the experimental radiance ratios for both narrowband and broadband radiance measurements using chi-square optimization:

$$\begin{aligned} \chi^2(\lambda_m, T_1, T_2) = &\left(\frac{\beta_1^{model}(\lambda_m, T_1, T_2)}{\beta_1^{exp}(\lambda_m, T_1, T_2)} - 1\right)^2 \\ &+ \left(\frac{\beta_2^{model}(T_1, T_2)}{\beta_2^{exp}(T_1, T_2)} - 1\right)^2 \end{aligned} \tag{20}$$

3. Synthetic double wavelength technique (SDWT)

DWT becomes competitive with absolute radiometric methods [13] as one ratio is measured with a narrow optical bandwidth while the other ratio is measured with a much broader spectral optical bandwidth [8]. DWT is very sensitive to the calibration of the relative spectral responsivities used in the measurements: an accuracy at 0.01% level is required. Such level of relative uncertainty can be reached only with a 'state-of-the-art' experimental set-up for the calibration of the relative spectral responsivity of the spectroradiometer used in the measurements, especially for large optical bandwidth (> 200 nm) which requires the use of an electrical substitution cryogenic radiometer [15]. Therefore, DWT is as complex and costly as absolute radiometric techniques [13]. This makes DWT unaffordable for a large number of national metrology institutes; which is not adequate for the '*mise-en-pratique*' of the new definition of the kelvin [2] and its dissemination.

For this reason, the authors have designed and validated a derivation of DWT named Synthetic Double Wavelength

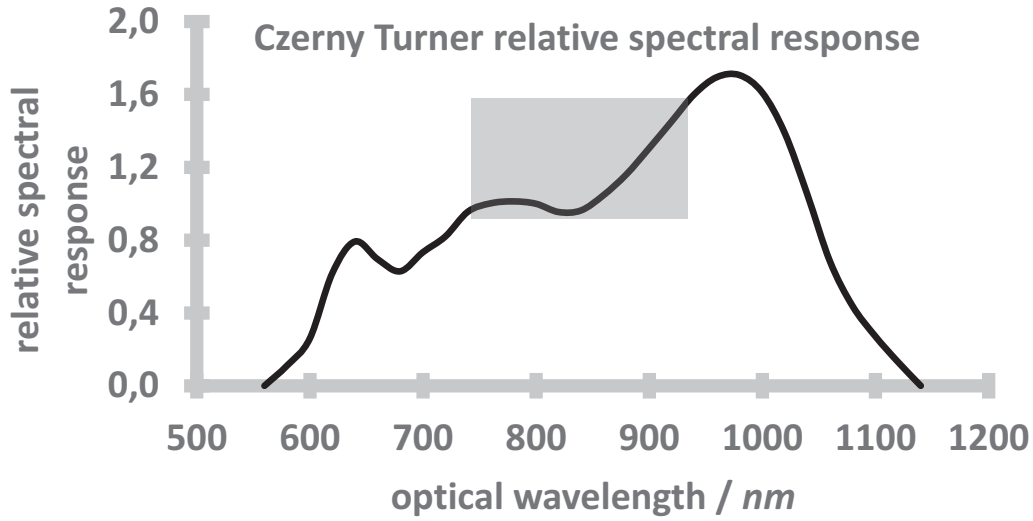

Figure 2. Relative (arbitrary units) spectral response $R(\lambda_m)$ of the spectroradiometer used in SDWT measurements.

Technique (SDWT). SDWT uses a tuneable spectroradiometer having a narrow optical bandwidth (few nm) for narrowband measurements. The broadband radiance measurement required in DWT is then simply computed using the recordings of sampled narrowband radiance measurements tuned over a large spectral range. If the relative optical responsivity of the tuneable spectroradiometer may be modelled over a broad spectral range, it can be calibrated with a reference white light source of known relative spectral radiance. This is exactly the case of Czerny-Turner monochromators which are commonly used in national metrology laboratories. This reference optical source may be simply an ITS-90 fixed point blackbody whose relative spectral radiance is known at 0.01% level. Here again, the experimental set-up is very common in any national metrology laboratory. Then SDWT may be a suitable technique for the realisation and the dissemination of thermodynamic temperature at high temperatures (above the copper fixed point) by a large number of NMIs.

3.1. SDWT principle and computation from measurement recordings

As stated above, the principle of SDWT is the same as for DWT but the broadband measurement of blackbody radiance is synthetized with narrowband measurements tuned over a wide optical spectrum range.

In our experimental set-up, the narrowband measurements of the blackbody radiance are performed with a Czerny-Turner simple monochromator at a chosen optical wavelength λ_m having an optical bandwidth of about 5 nm. Such narrow band optical detection can be considered as monochromatic in comparison to the blackbody spectral radiance (Planck's law). Thus, equations (5), (16) and (17) may be used to express the narrowband measurement equation (11):

$$\beta_1^{exp}(\lambda_m, T_1, T_2) = \frac{L(\lambda_m, T_2)}{L(\lambda_m, T_1)} \tag{21}$$

For the broadband signal, the measurement is performed with the same Czerny-Turner monochromator tuned from 730 nm to 930 nm (figure 2). The synthetic broadband ratio is computed from the narrowband photocurrents sampled over the broadband tuning range:

$$\beta_2^{exp}(T_1, T_2) = \frac{\sum_{i=1}^{N} I_1(\lambda_i, T_2)}{\sum_{i=1}^{N} I_1(\lambda_i, T_1)} \tag{22}$$

with $I_1(\lambda_i, T_1)$ and $I_1(\lambda_i, T_2)$ the photocurrent generated by the monochromatic measurement of the radiance of the blackbody at the temperature T_1 and T_2, respectively, performed with the Czerny-Turner monochromator whose slit scattering function is centered on the optical wavelength λ_i.

The expression of the photocurrent $I_1(\lambda_i, T)$ delivered by the Czerny-Turner monochromator can be expressed with the equation (15). Therefore, the expression of the synthetic (broadband) radiances ratio equation (10) becomes simpler:

$$\beta_2^{model}(T_1, T_2) \cong \frac{\sum_{i=1}^{N} [R(\lambda_i) \cdot L(\lambda_i, T_2)]}{\sum_{i=1}^{N} [R(\lambda_i) \cdot L(\lambda_i, T_1)]} \tag{23}$$

This expression is the same model as used for the DWT, replacing analytic spectral integration by numerical spectral integration.

For comparison to DWT, the equivalent synthetic spectral responsivity used in SDWT (figure 3) has been computed for N = 101 recorded samples (narrowband measurement of blackbody radiance) sampled over a broadband optical spectrum ranging from $\lambda_{(i=1)} = 730\,\text{nm}$ to $\lambda_{(i=N)} = 930\,\text{nm}$. Each narrowband measurement having an optical bandwidth of about $\Delta = 5$ nm.

Unlike the case of monochromatic/infinite bands described in section 2, the temperature dependence of the narrowband and the broadband measurements of radiance ratios are therefore very close and the two equations system (equations (11) and (12)) used in SDWT are only slightly different; making the thermodynamic temperatures T_1 and T_2 very sensitive to

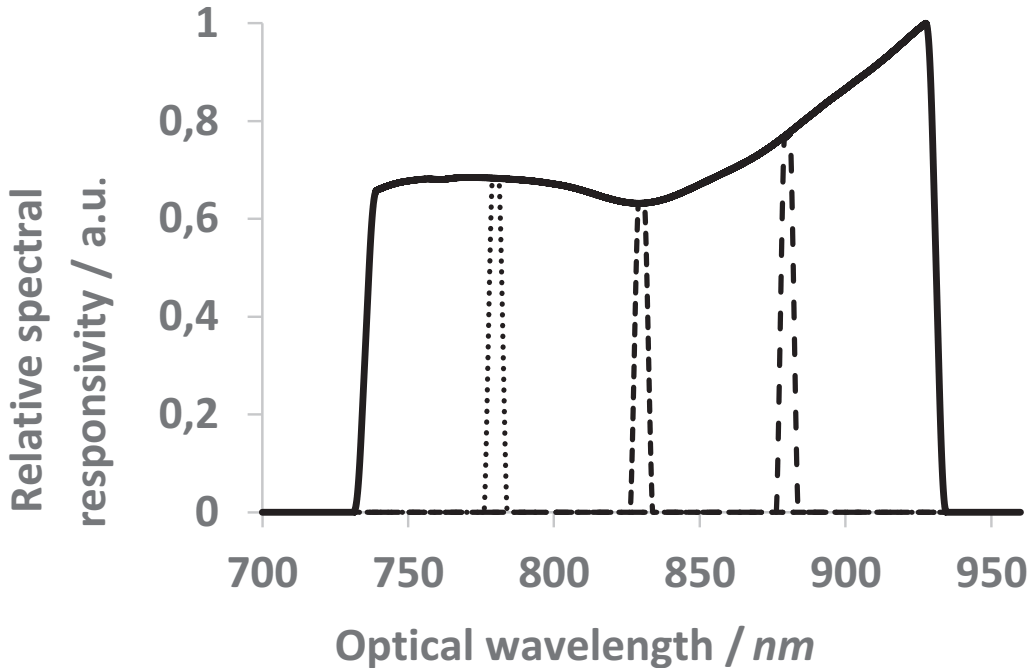

Figure 3. Solid line: synthetic relative spectral responsivity obtained by scanning the Czerny-Turner monochromator over the spectral range from 730 nm to 930 nm. Different dot lines: relative spectral responsivity of the Czerny-Turner monochromator with optical bandwidth about 5 nm for different measurement wavelength λ_i= 780 nm, 830 nm or 880 nm.

noise or to any systematic effects. Further measurements will be performed with larger spectral range for improvement of SDWT sensitivity.

Therefore, a numerical solution of this problem becomes far from simple. In this configuration, chi-square surface (equation 20) has the shape of a tiny valley surrounded by very steep mountains on each side but exhibiting a very flat bottom level.

In our experimental set-up (Czerny-Turner monochromator), the optical bandwidth of the measurements of blackbody radiance is sufficiently narrow (5 nm) to use equation (17) while keeping computation errors below 10 mK. In this approximation, equation (21) is valid and may be used to derive an analytical expression of temperature T_1 as a function of the temperature T_2 and the narrowband optical wavelength λ_i:

$$T_1 = \frac{C_2}{n(\lambda_m)\cdot\lambda_m\cdot ln\left\{1+\beta_1^{exp}(T_1,T_2,\lambda_m)\left[e^{\frac{C_2}{n(\lambda_m)\cdot\lambda_m\cdot T_2}}-1\right]\right\}} = g(\lambda_m,T_2) \tag{24}$$

Replacing the analytic expression of the thermodynamic temperature T_1 (24), in the analytic expression of the synthetic broadband ratio (23) gives a final measurement equation (25) which depends only on the single temperature T_2 and on the narrowband optical wavelength λ_m:

$$\beta_2^{model}(T_1,T_2) \to \beta_2^{model}(\lambda_m,T_2) \cong \frac{\sum_{i=1}^{N}[R(\lambda_i)\cdot L(\lambda_i,T_2)]}{\sum_{i=1}^{N}[R(\lambda_i)\cdot L(\lambda_i,g(\lambda_m,\mathrm{T_2}))]} \tag{25}$$

The synthetic broadband measurement equation (12) may then be solved with chi-square optimization to find a numerical value of the thermodynamic temperature T_2:

$$\chi^2(T_2,\lambda_m) = \left(\frac{\beta_2^{model}(\lambda_m,T_2)}{\beta_2^{exp}(T_1,T_2)}-1\right)^2 \tag{26}$$

The value of the temperature T_1 may then be deduced from equation (24), using numerical values for T_2 and λ_m.

4. Measurement of blackbody temperature with ITS-90 scheme over the range 730 nm to 930 nm

The low temperature blackbody used in SDWT measurements is the LNE-Cnam copper fixed-point blackbody used as the national reference. Its temperature T_1 is defined in the ITS-90 (T_{Cu}) [16]. It has been fully characterized in past studies [17, 18]. The goal of this paper is the experimental proof of principle of SDWT. The choice of an ITS-90 reference blackbody (here copper fixed point) as one of the two studied blackbodies allows for a simple and robust validation scheme of SDWT. Following this choice, the scale temperatures of the two blackbodies are known. The low temperature blackbody has then the scale value $T_1(\lambda_m) = 1357.77\,\mathrm{K}$ while the scale value of the high temperature blackbody is computed at any optical wavelength λ_m, including any spectral systematic effects.

The high temperature blackbody is a Re-C eutectic fixed point cell which has been fully characterised in previous papers [19, 20] as well as thermal gradients coming from the furnace and the cell design. In this paper, the temperature of

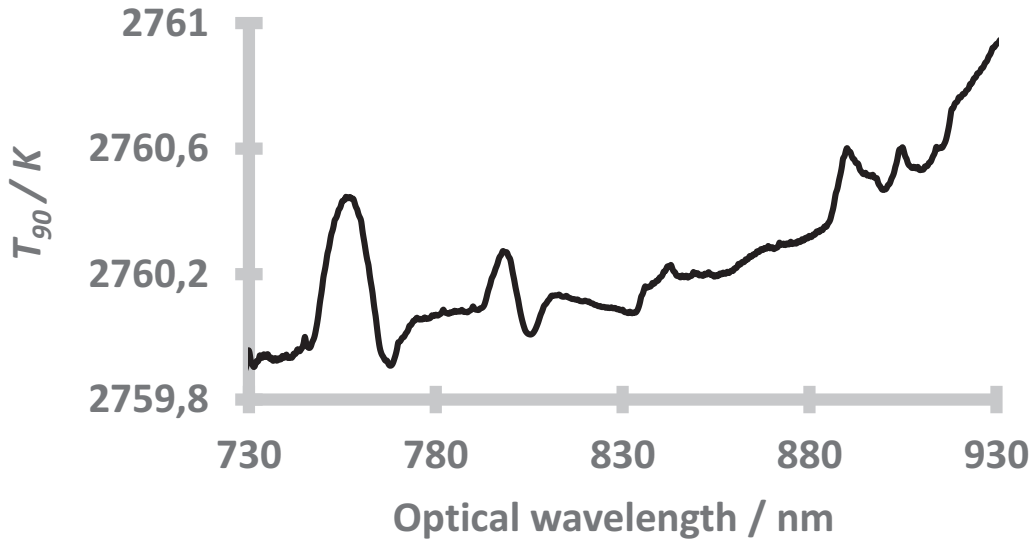

Figure 4. Temperature scale $T_{90}(\lambda_m)$ computed from experimental datas (scan of the optical wavelength for each black body).

the Re-C blackbody was fixed slightly above (2760 K) the liquidus temperature (2748 K) thanks to a feedback-loop reacting on the supply current of the oven electrical heater.

At LNE-Cnam, the spectroradiometer used for narrowband measurements images the blackbody output on the input slit of a Czerny-Turner simple monochromator used as a tuneable spectral filter. An argon spectral lamp was used for the calibration of the central optical wavelength of the 1st order optical diffraction slit scattering function of this simple monochromator.

The calibration of the relative spectral response $R(\lambda_m)$ (see figure 2) of the spectroradiometer may be realized by any way with a radiometric reference (like a tunable narrowband optical source together with a flat spectral response photodetector). For the proof of concept of SDWT and for simplicity, the relative spectral response $R(\lambda_m)$ of our spectroradiometer has been calibrated with our ITS-90 copper fixed-point blackbody reference ($T_{Cu} = 1357.77\,\mathrm{K}$) according equation (27), within the approximation of a narrowband optical measurement (15):

$$R(\lambda_m) = \frac{I_1(\lambda_m, T_{Cu})}{L(\lambda_m, T_{Cu})} \tag{27}$$

The choice of the use of an ITS-90 fixed point for the calibration of the relative spectral responsivity of our spectroradiometer has to be limited to the demonstration of the proof of concept of SDWT. Whereas a blackbody reference is used for the calibration of the spectral responsivity of our spectroradiometer, it would be easier and more accurate to use narrowband ratio for extrapolation of the thermodynamic temperature of the Re-C blackbody from the thermodynamic temperature of the ITS-90 fixed point.

The freezing plateau on the Cu point was flat within few mK over the complete measurement duration (one hour). The error introduced by using ITS-90 temperature value of the Cu point (1357.77 K) instead of its thermodynamic temperature (1357.80 K) taken from last radiometric determination [13] is about 0.12 K around 2760 K.

The temperature $T_2 = T_{90}$ of the high temperature blackbody can therefore be expressed in the ITS-90 using the narrowband measurement equation (21) together with Planck's law (equation 5).

$$T_{90}(\lambda_m) \cong \left[\frac{C_2}{n(\lambda_m)\cdot\lambda_m}\right] \cdot \frac{1}{ln\left[1 + \frac{e^{\frac{C_2}{n(\lambda_m)\cdot\lambda_m\cdot T_{Cu}}} - 1}{\beta_1^{exp}(\lambda_m, T_{Cu}, T_{90})}\right]} \tag{28}$$

The scale temperature T_{90} of the high temperature blackbody was computed at each optical wavelength (λ_m) tuned over a broadband spectral range (from 730 nm to 930 nm). These measurements are summarised in figure 4. Instead of finding the same temperature at each measurement optical wavelength, the measured temperatures $T_{90}(\lambda_m)$ exhibit strong spectral variation as may be seen on the figure.

The scan of the optical wavelength (from 730 nm to 930 nm) was repeated to check the repeatability of the curve $T_{90}(\lambda_m)$ (figure 4). The difference between these two scans is reported on figure 5. It remains negligible: below 20 mK (excepted around 767 nm). The strong spectral variations observed on $T_{90}(\lambda_m)$ (figure 4) are therefore reproducible. In conclusion, this systematic effect is most likely to be caused by our spectroradiometer (a simple Czerny-Turner monochromator) used for the measurements of the radiance of both blackbodies.

At this stage, it is important to mention that simple Czerny-Turner monochromators are usually used with a high pass filter to suppress optical flux coming from the second diffraction order generated by the optical Bragg grating. As no optical filter were used in our experiments, second order optical diffraction may cause partly the systematic spectral variations observed in $T_{90}(\lambda_m)$.

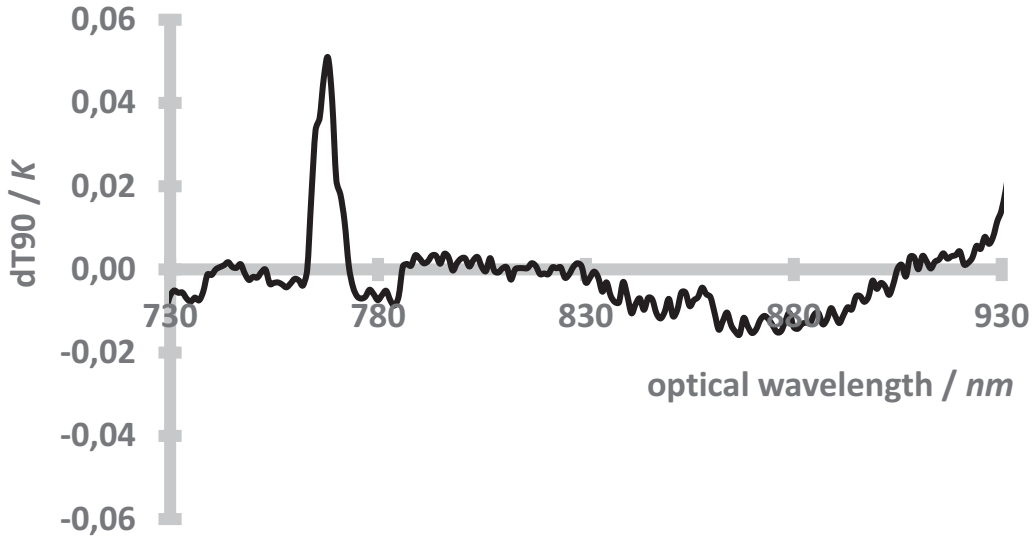

Figure 5. Temperature difference ($dT_{90}(\lambda_m)$) of the scale temperature of the high temperature blackbody computed for each of the two repeated optical wavelength scans.

At 1358 K, the blackbody radiance diffracted in the second order remains negligible (< 0.02 %) in comparison to the first order diffracted radiance from 730 nm to 930 nm (first-order optical wavelength). While at 2760 K, the ratio of second-order to first-order blackboy radiance diffracted is no more negligible: it can raise up to 10% at 930 nm. The detection of the optical flux coming from the optical diffraction in the second order may explain partly the spectral variations observed on $T_{90}(\lambda_m)$.

Out-of-band optical stray light [21] is another systematic effect which may explain the spectral variations observed on $T_{90}(\lambda_m)$. It originates from optical diffusion inside the monochromator. For the narrowband measurement of blackbody radiance, this error is maximum at low temperature and at shorter-wavelength. Out-of-band stray light may explain the error observed in the shorter wavelength part of the blackbody spectral radiance measured. Usually, out-of-band stray light is suppressed using an interference band pass optical filter. Nevertheless, SDWT requires a large scan of the optical wavelength while interference bandpass filter may not be tuned. We expect associating a tunable bandpass optical filter to our set-up in next future (Lyot, Acousto-Optic, MEMS, liquid crystal).

From Wien's law (equation 18) one may compute easily the following sensitivities, useful for uncertainty computation:

$$\left[\frac{dT_{90}}{T_{90}}\right] / \left[\frac{dL(\lambda,T_{90})}{L(\lambda,T_{90})}\right] \cong \frac{\lambda \cdot T_{90}}{C_2} \tag{29}$$

$$\left[\frac{dT_{90}}{T_{90}}\right] / \left[\frac{d\lambda}{\lambda}\right] \cong \frac{T_{90}}{T_{Cu}} - 1 \tag{30}$$

The uncertainty budget of temperature measurements realized using ITS-90 scheme is strongly dominated by the spectral systematic effects observed in the curve $T_{90}(\lambda_m)$ (98%) see table 1.

The average scale temperature has been computed: $T_{90}(\lambda)_{730\,\mathrm{nm}}^{930\,\mathrm{nm}} = 2760.25\,\mathrm{K}$.

As a conclusion, in our case, one can fully neglect usual uncertainty components in comparison to the spectral systematic effects observed which are caused by our spectroradiometer. These effects need to be studied in detail and this investigation is out of the scope of this article whose goal is the demonstration of the feasibility of SDWT and the investigation of its potential for the *mise-en-pratique* of the kelvin.

5. Determination of blackbody thermodynamic temperature with SDWT from 730 nm to 930 nm

The thermodynamic temperatures $T_1(\lambda)$ and $T_2(\lambda)$ of our blackbodies have been determined using the SDWT at any monochromatic optical wavelength λ_m from 730 nm to 930 nm (see figures 6 and 7). The spectral variations observed on $T_{90}(\lambda_m)$ measurements are larger with SDWT, as it is much more sensitive to signal and spectral errors than the ITS-90 scheme. SDWT sensitivity was estimated from Monte Carlo simulations.

Thanks to the conclusions on scale temperature measurements, SDWT uncertainty budget was focussed on the three most important uncertainty components: sensitivity to the blackbody radiance and to the optical wavelength. The sensitivity of SDWT to these uncertainty components has been deduced from Monte Carlo simulation after introducing random noise on the blackbody radiances or on the measured optical wavelength. In our measurement configuration (narrowband and broadband measurement optical bandwidths described in figure 3), and for our blackbody temperatures (about 1358 K and 2760 K), the sensitivity of SDWT to radiance deviations is about 30 times larger than ITS-90 sensitivity to this parameter (see figures 8 and 9) and the sensitivity of SDWT to optical wavelength deviations is about 20 times larger than ITS-90 sensitivity to optical wavelength (see figures 10 and 11). This explains why systematic spectral effects observed on SDWT temperature values are much more important than those observed on ITS-90 temperature values.

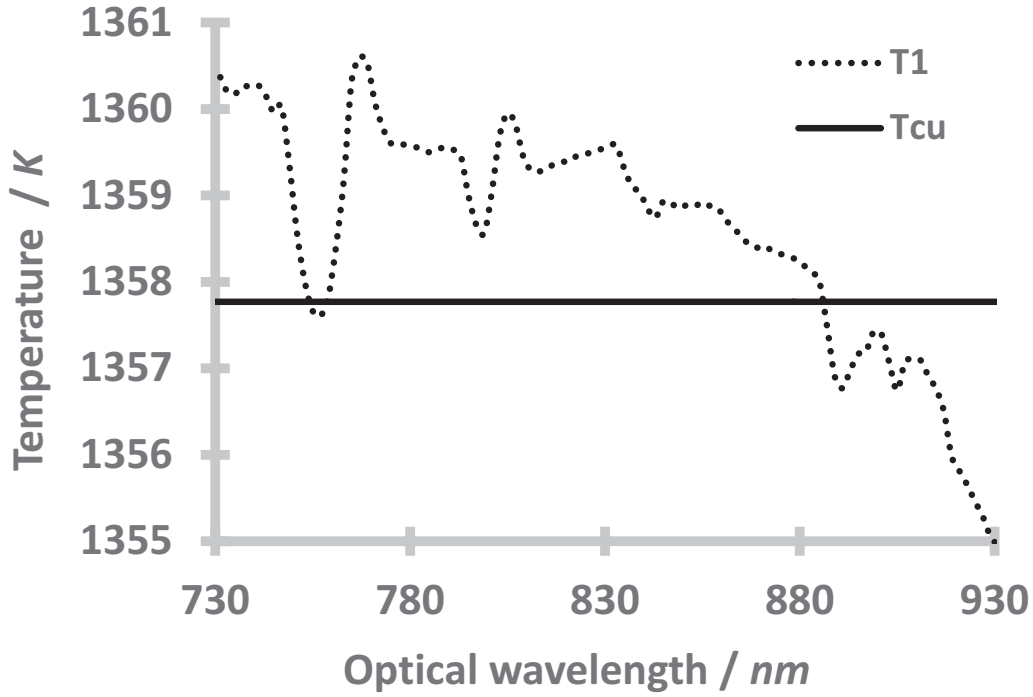

Figure 6. Thermodynamic temperature $T_1(\lambda_m)$, calculated with SDWT (dot line) and in scale temperature $T_{90}(\lambda_m)$ (solid line, fixed value T_{cu}) for different narrowband measurement optical wavelengths λ_m.

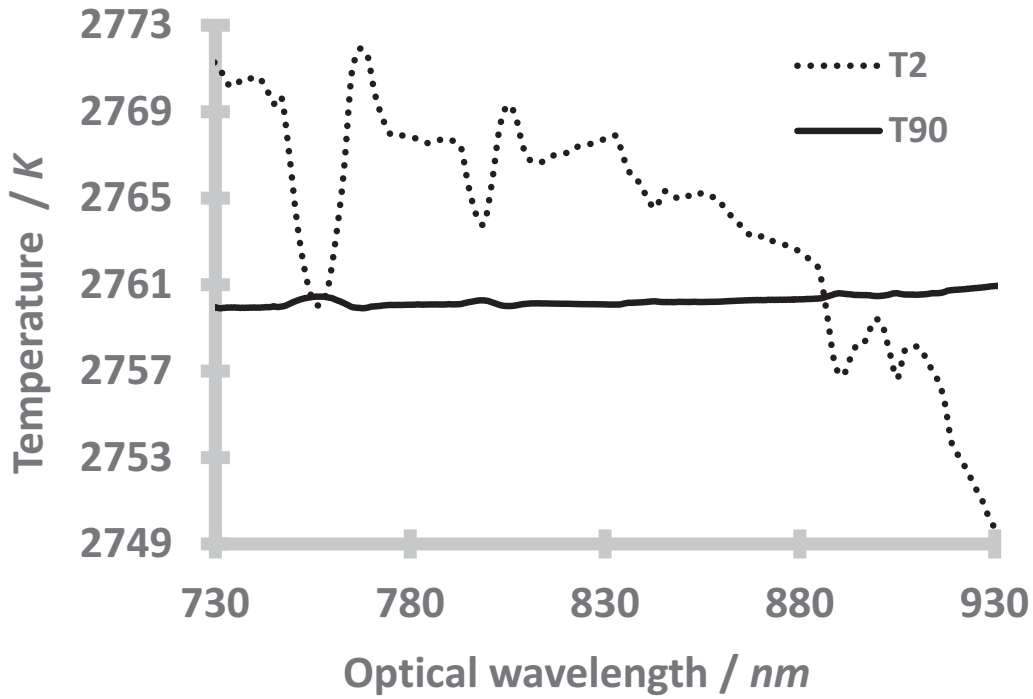

Figure 7. Thermodynamic temperature $T_2(\lambda_m)$ calculated with SDWT (dot line) and in scale ITS-90 (solid line, $T_{90}(\lambda_m)$) for different narrowband measurement optical wavelengths λ_m.

As for ITS-90, SDWT uncertainty budget is strongly dominated by the systematic spectral effects. In the absence of such spectral systematic effects, the standard uncertainty should be about 0.40 K at 1358 K and 2 K at 2760 K making SDWT a very simple and efficient technique for the determination of thermodynamic temperature with usual radiometry equipment easily affordable.

6. Systematic errors

Spectral optical detection errors are dominant in SDWT. Their investigation was performed using numerical simulations based on our knowledge of our instrument (Czerny Turner simple monochromator) and on previous studies.

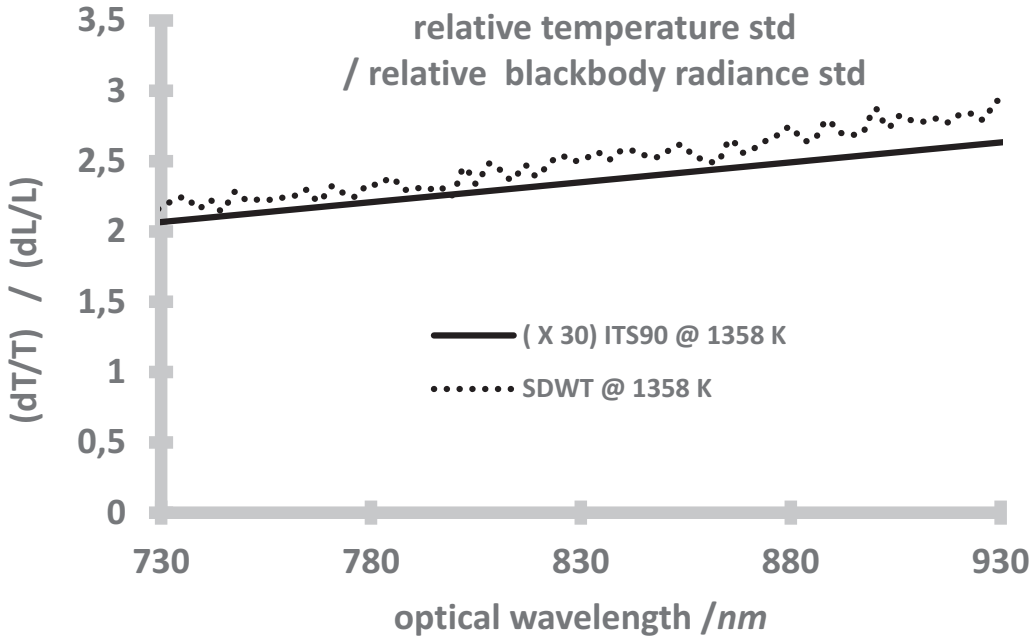

Figure 8. Sensitivity of temperature fluctuations T_1 with blackbody radiance fluctuations. Computation for both SDWT (dot line) and in the ITS-90 scheme (solid line, T_{90}) temperatures over a broad range of narrowband optical wavelengths λ_m.

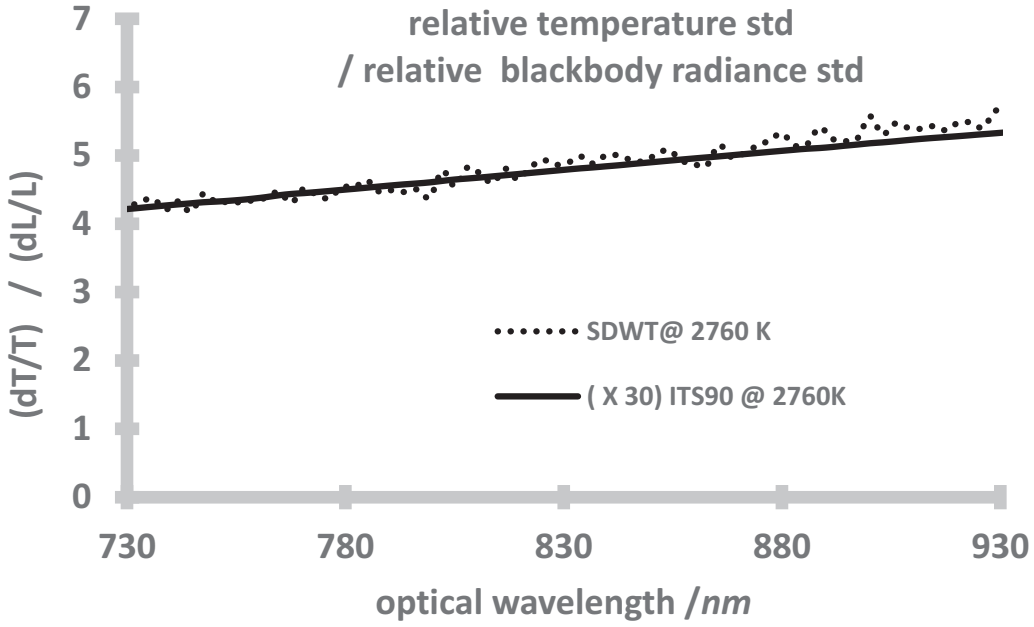

Figure 9. Sensitivity of relative standard deviation on temperature T_2 with relative standard deviation on measured blackbody radiance. Computation for both SDWT (dot line) and in scale ITS-90 (solid line, T_{90}) temperatures over a broad range of narrowband optical wavelengths λ_m.

6.1. Out-of-band stray light (optical diffusion)

In the presence of optical diffusion, the spectral responsivity of the monochromator ($S_1(\lambda,\lambda_m)$, equation 13) is replaced by $S_{OOB}(\lambda,\lambda_m)$:

$$S_{OOB}(\lambda,\lambda_m) = R(\lambda_m)\cdot\delta(\lambda-\lambda_m) + D(\lambda) \qquad (31)$$

with $D(\lambda)$ the component of the spectral responsivity of the monochromator caused solely by optical diffusion.

Therefore, out-of-band stray light becomes part of the expression of the narrowband photocurrent $I_1(\lambda_m,T)$:

$$I_1(\lambda_m,T) = k_1\int_0^\infty S_{OOB}(\lambda,\lambda_m)\cdot L(\lambda,T)\,d\lambda = k_1\cdot R(\lambda_m)\cdot L(\lambda_m,T)\cdot[1+OOB(\lambda_m,T)] \qquad (32)$$

with out-of-band stray light defined by equation (33):

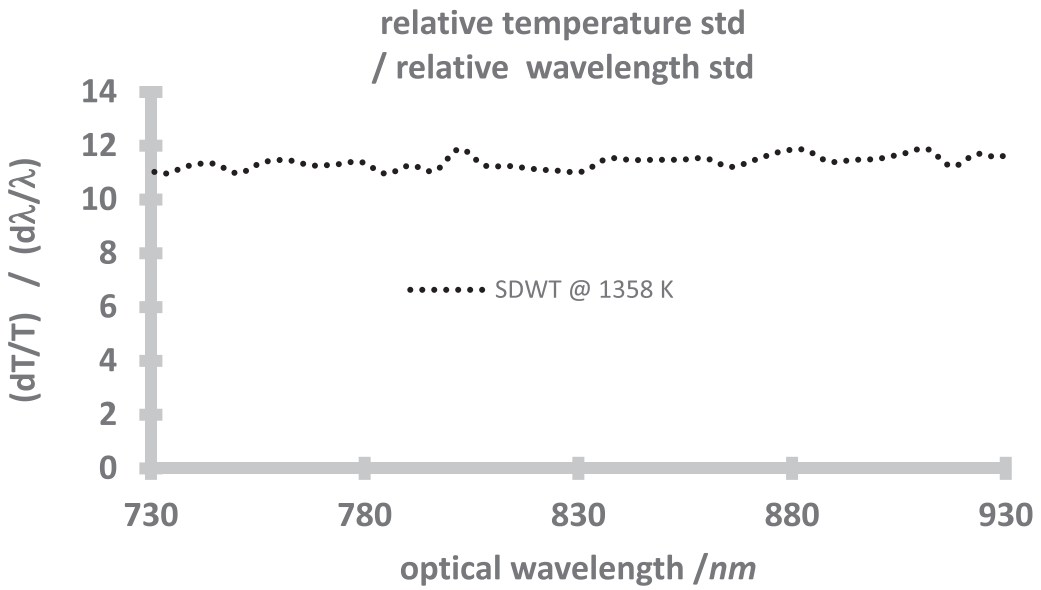

Figure 10. Sensitivity of relative standard deviation on temperature T_1 with relative standard deviation on optical wavelength. Computation for SDWT over a broad range of narrowband optical wavelengths λ_m.

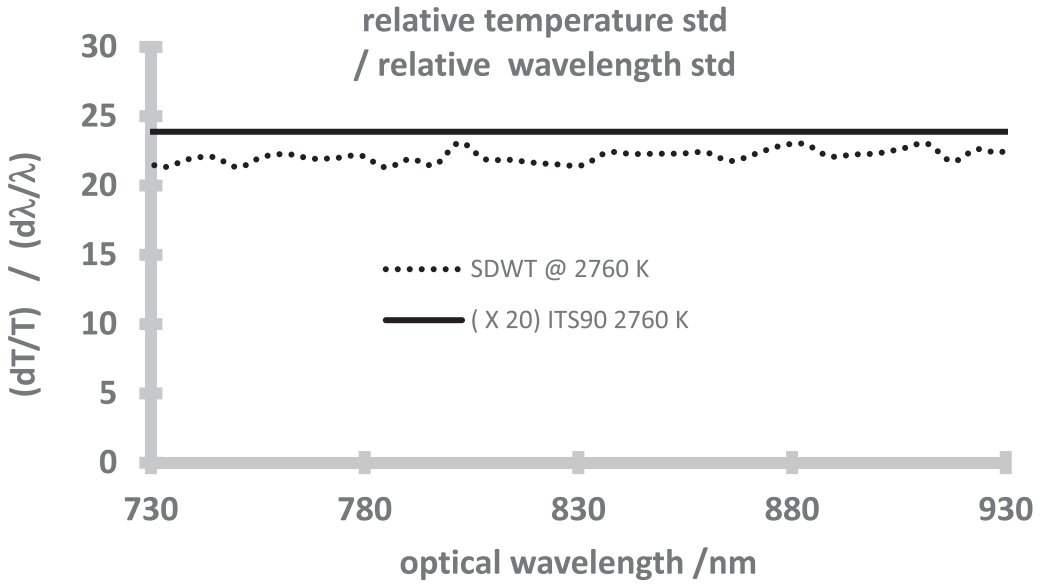

Figure 11. Sensitivity of relative standard deviation on temperature T_2 with relative standard deviation on optical wavelength. Computation for both SDWT (dot line) and in scale ITS-90 (solid line, T_{90}) over a broad range of narrowband optical wavelengths λ_m.

$$OOB(\lambda_m, T) = \frac{\int_{\lambda_{UV}^{Si}}^{\lambda_{IR}^{Si}} D(\lambda) \cdot L(\lambda, T)\, .d\lambda}{R(\lambda_m) \cdot L(\lambda_m, T)} \tag{33}$$

The model taken for optical diffusion is very simple: the optical diffusion background ($D(\lambda)$) is proportional to the spectroradiometer spectral response ($R(\lambda)$):

$$D(\lambda) = D_0 \cdot R(\lambda) \tag{34}$$

with $D_0 = 5{\cdot}10^{-7}\,\mathrm{nm}^{-1}$.

This very simple optical diffusion model yields an error on T_{90} of about -0.1 K at 2760 K which was measured at the optical wavelength 808 nm using a notch filter. This correction is much larger for temperatures T_1 and T_2 determined with SDWT, thanks to its high sensitivity to radiance deviations compared to T_{90}. It is important at this stage to observe that the out-of-band error is larger in the shorter wavelength range of the optical spectrum.

SDWT presents a 'magical' optical wavelength (λ_{OOB}) for which the out-of-band errors at the two temperatures T_1 and T_2 cancels out.

This may be easy to understand in the case of Double Wavelength Technique as one may assume in a good approximation that out-of-band affects much more narrowband radiance measurements than broadband radiance measurements. Following this assumption and using our simple optical diffusion model (equation 33), the out-of-band error only affects the narrowband ratio of blackbody radiances

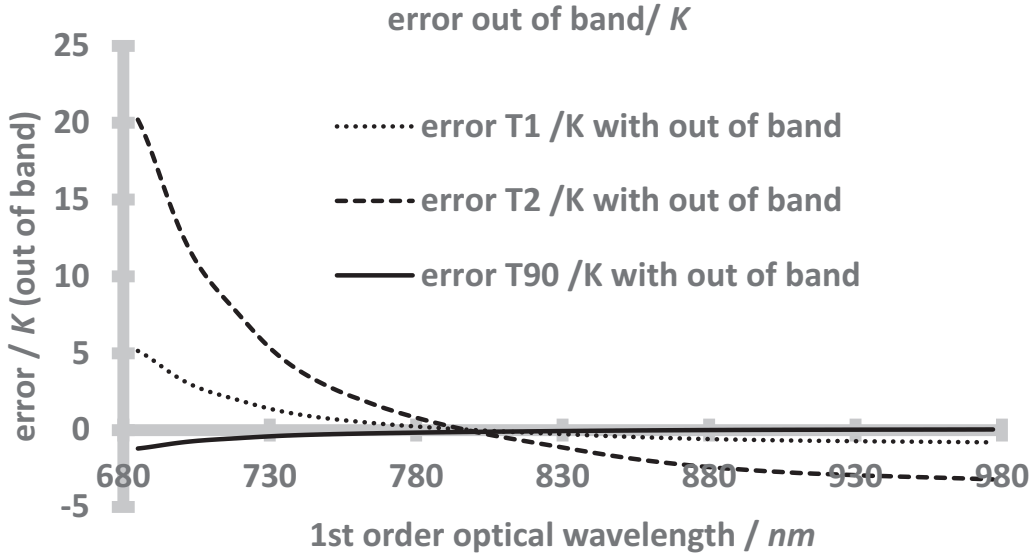

Figure 12. Out-of-band error (optical diffusion) simulated for each temperature computed (T_1, T_2 and T_{90}) at each measurement optical wavelength.

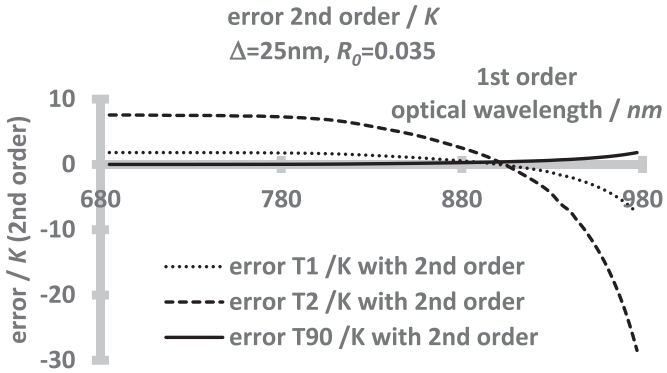

Figure 13. Optical Bragg diffraction error (2nd order) simulated for each temperature computed (T_1, T_2 and T_{90}) at each measurement optical wavelength.

measured at temperatures T_1 and T_2 which remains unchanged if the following condition is fulfilled:

$$\frac{L(\lambda_{OOB}, T_2)}{L(\lambda_{OOB}, T_1)} = \frac{\int D(\lambda) \cdot L(\lambda, T_2) \cdot d\lambda}{\int D(\lambda) \cdot L(\lambda, T_1) \cdot d\lambda} \tag{35}$$

In the case of SDWT, the computation of this magic optical wavelength is rather more complicated. As the broadband synthetic signals result from a summation of the measured narrowband optical radiances, the out-of-band error is no more negligible for the synthetic broadband ratio, unlike DWT case. Nevertheless, numerical computations also demonstrate the existence of such magic wavelength for SDWT ($\lambda_{OOB} \cong$ 800 nm in our experimental configuration, see figure 12). This wavelength is then interesting as it is not sensitive to this type of out-of-band error.

6.2. Second order Bragg optical diffraction

The resonant optical wavelength of the second order optical Bragg diffraction is simply the half of the resonant optical wavelength of the first order optical Bragg diffraction. As first order optical wavelength is tuned from $\lambda_{\min} = 680$ nm to $\lambda_{\max} = 980$ nm in SDWT, the second order optical wavelength covers the range $\frac{\lambda_{\min}}{2} = 340$ nm to $\frac{\lambda_{\max}}{2} = 490$ nm, below the wavelength range used for the recording of the optical spectral responsivity of our Czerny Turner monochromator (figure 2). The monochromatic spectral responsivity $S_1(\lambda, \lambda_m)$ of the monochromator is modified to include second order optical Bragg diffraction. It is then replaced by $S_B(\lambda, \lambda_m)$:

$$S_B(\lambda, \lambda_m) = R(\lambda_m) \cdot \delta(\lambda - \lambda_m) + R\left(\frac{\lambda_m}{2}\right) \cdot \delta\left(\lambda - \frac{\lambda_m}{2}\right) \tag{36}$$

Therefore, second order Bragg optical diffraction becomes part of the expression of the narrowband photocurrent $I_1(\lambda_m, T)$:

$$\begin{aligned} I_1(\lambda_m, T) &= k_1 \int_0^\infty S_B(\lambda, \lambda_m) \cdot L(\lambda, T)\, d\lambda \\ &= k_1 \cdot R(\lambda_m) \cdot L(\lambda_m, T) \cdot \left[1 + Bragg^{(2)}(\lambda_m, T)\right] \end{aligned} \tag{37}$$

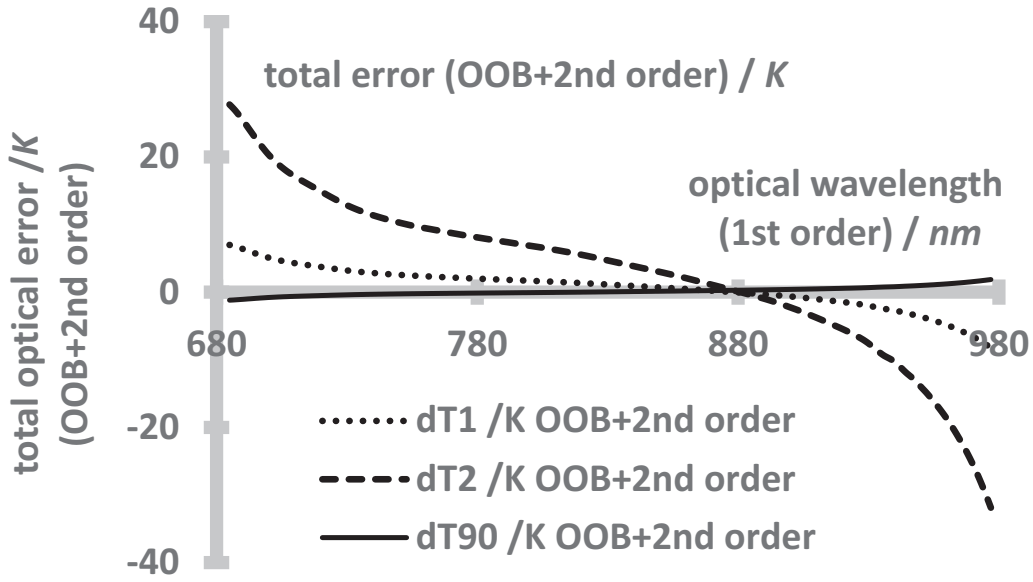

Figure 14. Total optical detection error (optical diffusion and second order Bragg optical diffraction) simulated for each temperature computed ($T_1(\lambda_m)$, $T_2(\lambda_m)$ and $T_{90}(\lambda_m)$) at each measurement optical wavelength λ_m for the narrowband ratio.

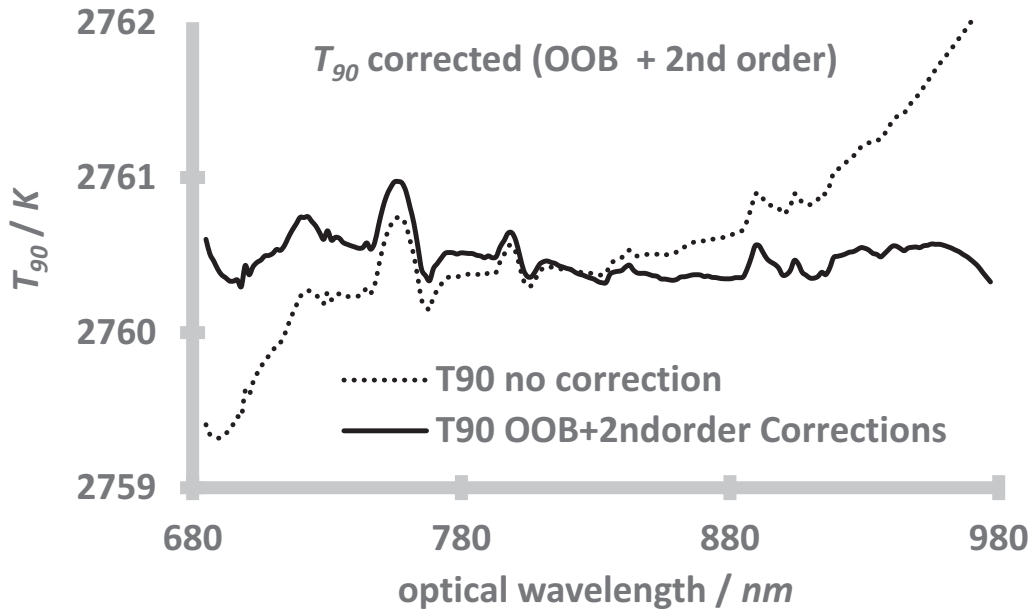

Figure 15. Comparison of $T_{90}(\lambda_m)$ (ITS-90) with and without correction of optical detection errors. Total optical detection error (addition of optical diffusion and optical diffraction) is simulated.

with second order Bragg optical diffraction defined by equation (38):

$$Bragg^{(2)}(\lambda_m, T) = \frac{R(\lambda_m/2)\cdot L(\lambda_m/2, T)}{R(\lambda_m)\cdot L(\lambda_m, T)} \tag{38}$$

The spectral responsivity of the monochromator has not been measured below 490 nm. Therefore, it has been modelled with a simple decay rate related to the spectral responsivity of the silicon photodiode used in optical detection, but also related to the spectral reflectivity of the gold mirrors of our monochromator.

For $340\,\text{nm} \leq \lambda \leq 490\,\text{nm}$, the spectral response $R(\lambda)$ of the monochromator has been simulated with the following model:

$$R(\lambda) = R_0 \cdot e^{\left(\frac{\lambda - \lambda_{max}/2}{\Delta}\right)} \tag{39}$$

For $680\,\text{nm} \leq \lambda \leq 980\,\text{nm}$, the spectral response $R(\lambda)$ of the monochromator has been determined with radiance measurement of the ITS-90 copper fixed point blackbody (figure 2, equation 27).

The detected optical flux which comes from the second order optical Bragg diffraction gives a rather small error on T_{90} (about 0.050 K) at the optical wavelength 808 nm. This

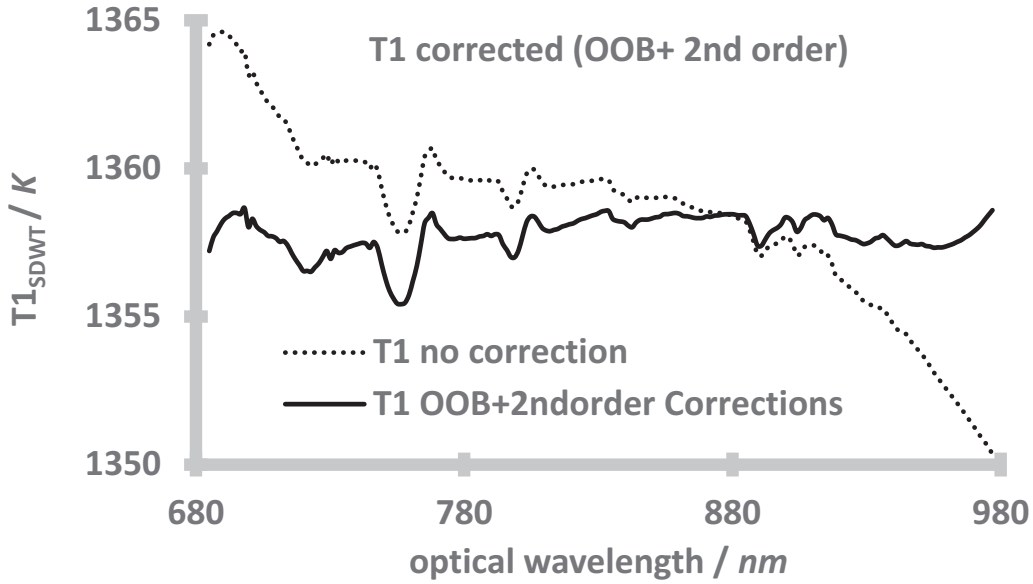

Figure 16. Comparison of $T_1(\lambda_m)$ (SDWT) with and without correction of optical detection errors. Total optical detection error (addition of optical diffusion and optical diffraction) is simulated.

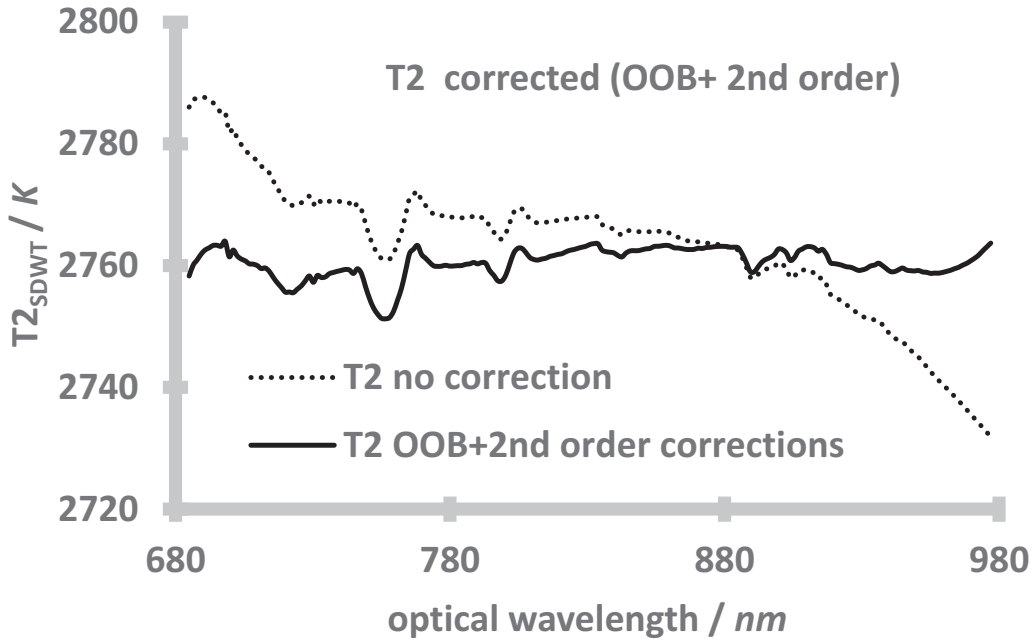

Figure 17. Comparison of $T_2(\lambda_m)$ (SDWT) with and without correction of optical detection errors. Total optical detection error (addition of optical diffusion and optical diffraction) is simulated.

correction is much larger for temperatures T_1 and T_2 determined with SDWT, thanks to its high sensitivity to radiance deviations compared to T_{90}. This optical diffraction error is also flat in the shorter wavelength range of the optical spectrum (see figure 13).

As well as for out-of-band error, one can find a 'magical' optical wavelength (λ_{2nd}) for which the second order optical Bragg diffraction errors at the two temperatures T_1 and T_2 cancels out. In our experimental configuration, $\lambda_{2nd} \cong 905$ nm. This optical wavelength is then interesting as it is not sensitive to second order optical Bragg diffraction error.

6.3. Total optical corrections

As a conclusion the total optical error (addition of out-of-band error and second order optical Bragg diffraction error) has been simulated for T_1, T_2, T_{90} (figure 14). SDWT and ITS-90 schemes both present a 'magical' optical wavelength (around 880 nm for SDWT and around 820 nm for ITS-90) for which the total optical error is zero.

The scale temperature $T_{90}(\lambda_m)$ has been corrected for these optical detection errors (figure 15). The shorter wavelength and IR slopes are then correctly cancelled but the sharp

Table 1. T_{90} uncertainty budget @ 2760.25 *K*.

Component *(C)*	*u(C)*	Unit	Sensivitity	Sensitivity unit	$u(T_{90})$/K
Czerny-Turner spectroradiometer					**0.58**
Optical wavelength	1.0E-02	nm	3.53	K/nm	0.036
Size of source effect	1.0E-04	-	424	K	0.042
Linearity of optical detection	5.0E-05	-	424	K	0.021
Out-of-band optical flux	5.0E-05	-	424	K	0.021
Gain ratio Voltage to Current Amp.	7.0E-05	-	424	K	0.030
Systematic spectral errors	5.8E-01	K	1.00	-	0.58
Copper fixed point blackbody					**0.051**
Impurities	5.0E-03	K	4.13	-	0.021
Emissivity, thermal leaks	5.0E-03	K	4.13	-	0.021
Plateau identification	2.0E-03	K	4.13	-	0.008
Repeatability	1.0E-02	K	4.13	-	0.041
High Temperature blackbody					**0.044**
Emissivity, thermal leaks	1.0E-04	-	424	K	0.043
Stability	1.0E-02	K	1	-	0.010
$u(T_{90})$/K					**0.59**

Table 2. SDWT uncertainty budget (simplified, thanks to T_{90} uncertainty budget analysis).

component *(C)*	Uncertainty u*(C)*	unit	Sensitivity	Sensitivity unit	Temperature uncertainty/K
$u(T_{SDWT})$ *@ 1358* K					**2.9**
Signal relative uncertainty	1.0E-04	-	3400	K	0.34
Optical wavelength uncertainty	1.0E-02	nm	19	K	0.19
Spectral systematic effects	2.9	K	1	-	2.90
$u(T_{SDWT})$ *@ 2760* K					**13**
Signal relative uncertainty	1.0E-04	-	13 500	K	1.4
Optical wavelength uncertainty	1.0E-02	nm	75	K	0.8
Spectral systematic effects	13	K	1	-	13

spectral variations are still present. The same conclusions may be applied to the temperatures $T_1(\lambda_m)$ and $T_2(\lambda_m)$ determined with SDWT (figures 16 and 17).

The simulated optical corrections presented in figure 14 have been applied to the thermodynamic temperatures $T_{90}(\lambda_m)$, $T_1(\lambda_m)$ and $T_2(\lambda_m)$ (respectively figures 15–17).

Therefore, a spectral averaging of these corrected temperature values has been computed leading to the following mean values and standard deviations:

- $<T_1> = 1357.76$ K; $u(T_1) = 0.64$ K
- $<T_2> = 2760.5$ K; $u(T_2) = 2.5$ K
- $<T_{90}> = 2760.49$ K; $u(T_{90}) = 0.13$ K

Thanks to the optical corrections computed, the standard deviation coming from spectral variations has been approximately reduced by a factor 5 in comparison to non-corrected experimental values (uncertainty budgets detailed in tables 1 and 2).

Further improvements of the measurements using notch, bandpass and high pass spectral optical filters will be performed for the validation of the simulated optical corrections as well as for thermodynamic temperatures and attached uncertainties values presented in this section.

7. Conclusion

A new relative method named 'Synthetic Double Wavelength Technique' for the determination of thermodynamic temperature of blackbodies was studied and tested. This method only requires a tuneable (narrowband) spectroradiometer, a spectral lamp for its wavelength calibration and an ITS-90 fixed-point blackbody for its relative spectral responsivity calibration. Full computation of SDWT is presented. First measurements demonstrate the strong potential accuracy of SDWT despite systematic spectral effects were observed both on in-scale temperature and thermodynamic temperature determinations. These systematic errors come from the Czerny Turner simple monochromator used in the measurements of blackbody radiances. The use of an additional high-pass optical filter should suppress second order optical diffraction while a tunable bandpass optical filter would be required for the suppression of out-of-band stray light. A complete investigation of these systematic effects observed in our experimental set-up is planned in near future. Once these experimental defaults will be solved, SDWT shall provide a simple technique for the *Mise-en-Pratique* of the kelvin and its dissemination above 1234.93 K with an uncertainty potentially competitive with the best results achieved with absolute radiometric techniques

techniques. SDWT offers an alternative approach for national metrology laboratories which cannot afford an electrical substitution cryogenic radiometer for the *Mise-en-Pratique* of the new definition of the kelvin.

Acknowledgments

This work was carried out with funding from the Euramet EMPIR in the frame of the EMPIR JRP project 15SIB02 'Implementing the new kelvin 2—InK 2' and the national metrology programme of France.

References

[1] BIPM 2019 *The International System of Units (SI Brochure) 9th edn* (www.bipm.org/utils/common/pdf/si-brochure/SI-Brochure-9.pdf)
[2] BIPM 2019 *SI Brochure–Appendix 2 'Mise en pratique for the definition of the kelvin in the SI' 9th edn* (www.bipm.org/utils/en/pdf/si-mep/SI-App2-kelvin.pdf)
[3] Machin G, Engert J, Gianfrani L, McEvoy H and Sparasci F 2018 The european metrology programme for innovation and research project: implementing the new kelvin 2 (InK2) *J. Phys.: Conf. Ser.* **1065** 122002
[4] Wulfson K S 1951 Absolute method of blackbody temperatures measurement *J. Exp. Theor. Phys.* **21** (in Russian) pp. 507–9
[5] Sapritskii V I 1990 National primary radiometric standards of the USSR *Metrologia* **27** 53
[6] Prokhorov A V, Mekhontsev S N and Sapritsky V I 1999 *Proceedings of TEMPMEKO '99, 7th International Symposium on Temperature and Thermal Measurements in Industry and Science*, ed. Dubbeldam J F, de Groot M J pp. 567–72
[7] Woolliams E R, Winkler R, Salim S G R, Harris P M and Smith M I 2009 The double-wavelength technique—an alternative technique to determine thermodynamic temperature *Int. J. Thermophys.* **30** 144
[8] Saunders P 2014 Analysis of the potential accuracy of thermodynamic measurement using the double-wavelength technique *Int. J. Thermophys.* **35** 417
[9] Prokhorov A, Sapritsky V, Khlevnoy B and Gavrilov V 2015 Alternative methods of blackbody thermodynamic temperature measurement above silver point *Int. J. Thermophys.* **36** 252
[10] Ciddor P E 1996 Refractive index of air: new equations for the visible and near infrared *Appl. Opt.* **35** 1566
[11] Briaudeau S, Sadli M, Bourson F, Rougié B, Rihan A and Zondy J-J 2011 Primary radiometry for the mise-en-pratique: the laser-based radiance method applied to a pyrometer *Int. J. Thermophys.* **32** 2183
[12] Salim S G R, Briaudeau S, Bourson F, Rougié B, Truong D, Kozlova O, Coutin J-M and Sadli M 2016 A reference radiance-meter system for thermodynamic temperature measurements *Metrologia* **53** 945
[13] Woolliams E R *et al* 2016 Thermodynamic temperature assignment to the point of inflection of the melting curve of high temperature fixed points *Phil. Trans. R. Soc.* A **374** 20150044
[14] Woolliams E R, Dury M R, Burnitt T A, Alexander P E R, Winkler R, Hartree W S, Salim S G R and Machin G 2011 Primary radiometry for the mise-en-pratique for the definition of the kelvin: the hybrid method *Int. J. Thermophys.* **32** 1
[15] Martin J E, Fox N P and Key P J 1985 A cryogenic radiometer for absolute radiometric measurements *Metrologia* **21** 147
[16] Preston-Thomas H 1990 The international temperature scale of 1990 (ITS-90) *Metrologia* **27** 3
[17] Bourson F, Sadli M, Rougié B and Briaudeau S 2011 Study and comparison of newly developed ITS-90 silver- and copper-point cells *Int. J. Thermophys.* **32** 1602
[18] Bourson F, Sadli M, Rougié B, Briaudeau S and Kozlova O 2014 Influence of the opening of a blackbody cavity measured at the Ag and Cu ITS-90 fixed points *Int. J. Thermophys.* **35** 516
[19] Lowe D H *et al* 2017 The equilibrium liquidus temperatures of rhenium—carbon, platinum—carbon and cobalt—carbon eutectic alloys *Metrologia* **54** 390
[20] Sadli M, Anhalt K, Bourson F, Schiller S and Hartmann J 2009 Thermal effects in the HTBB-3200pg furnace on metal-carbon eutectic point implementation *Int. J. Thermophys.* **30** 69
[21] Keawprasert T, Anhalt K, Taubert D R and Hartmann J 2011 Monochromator-based absolute calibration of radiation thermometers *Int. J. Thermophys.* **32** 1697s